Model-Based Life Estimation of Li-ion Batteries in PHEVs Using Large Scale Vehicle Simulations: An Introductory Study

A. Di Filippi
Department of Mechanical Engineering
University of Salerno
84084 Fisciano (Salerno), Italy

S. Stockar, S. Onori, M. Canova, Y. Guezennec
Center for Automotive Research
The Ohio State University
Columbus, Ohio 43212, USA
Email: canova.1@osu.edu

***Abstract*—Plug-In Hybrid Electric Vehicles (PHEVs) are a promising mid-term solution to reduce the energy demand in the personal transportation sector, due to their ability of storing energy in the battery through direct connection to the electrical grid. However, an important aspect to a successful market acceptability for these vehicles is related to the reliability of the energy storage system.**

In this scenario, various studies have attempted at investigating the effects of current/power demand, calendar life and operating temperature on battery life, as well as estimating the residual life of the battery under various operating conditions.

This paper illustrates the preliminary results of a comprehensive study on Li-ion battery life estimation for PHEVs, predicting their residual life under real-world driving conditions. The methodology adopted is based on both deterministic and stochastic simulations to investigate the effects of electrical and thermal loading on the battery life. To this end, an electro-thermal battery model, inclusive of thermal dynamics and residual life estimation, is developed and utilized in conjunction with a vehicle model, a supervisory controller for PHEV energy management and real-world driving scenarios.

Within this framework, the proposed study addresses the impact of the PHEV control parameters on the battery life, namely the vehicle operating modes (charge depleting or charge sustaining), and constraints on the State of Charge (SoC).

I. Introduction

Plug-In Hybrid Electric Vehicles (PHEVs) are today considered a promising solution to reduce petroleum usage in the automotive transportation sector. The performance, cost and reliability of such vehicles is strongly driven by the energy storage system, for which the current state of the art is represented by Li-ion battery technology.

It is well known that electrochemical energy storage systems are subject to performance degradation due to the aging, which depends on various factors such as the current magnitude (C-rate), temperature, operating State of Charge (SoC) and calendar life. Such aspects are important over the lifetime of the vehicle and have been extensively studied through long term experiments on various battery technologies. However, most of the available information is based on results from laboratory testing, under very controlled environments, and using aging protocols which may not correctly reflect the actual vehicle utilization. Therefore, significantly differences in aging and battery life may exist when the batteries are utilized on a vehicle under specific operating conditions and usage patterns, leading to conservative vehicle designs where the battery system is typically oversized (hence more costly) to guarantee performance and range near the end of life.

However, studies on the estimation of battery life for Li-ion batteries in PHEV applications have acknowledged the importance of two aging factors, namely temperature and SOC/Depth of Discharge (DoD) [1], [2], [3], [4], [5]. Such factors are typically indirectly controlled or driven by the vehicle usage patterns, charging scenarios, battery pack sizing, vehicle control strategy, environmental factors and battery pack thermal management.

Leveraging on previous experimental battery aging studies, the proposed work presents the preliminary results of a simulation study of PHEVs to investigate the impact on battery life of a wide variety of usage scenarios and vehicle parameters. The study is based on a validated dynamic battery model based on an equivalent-circuit analogy, which integrates a dynamic thermal model that predicts the internal temperature in relation with the current demand and the boundary conditions. A characterization of battery aging based on the work presented in [3] is also included. Finally, the battery model is integrated into a vehicle model validated on a prototype PHEV mid-size SUV, which include a supervisory controller for energy management [6].

II. Overview of the Modeling Framework

Figure 1 shows the structure of the implemented battery model. The model is composed by three sub-models namely, electrical, thermal and aging models. The inputs of the system are the battery current, denoted as I_{batt}, and the ambient temperature T_{amb}. The model outputs are the battery voltage V and open circuit voltage V_{oc}, the battery temperature T and the severity factor σ, which is the key variable for battery life estimation [3].

A. Battery Electrical Model

The electrical model of the battery is based on a linear Randle equivalent circuit and is comprised of an open circuit

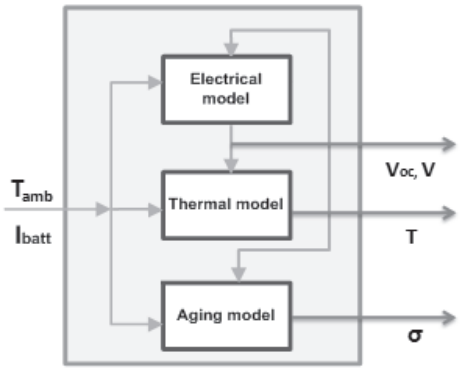

Fig. 1. Schematic of Battery Model Structure

voltage, an internal resistance R_0, and n parallel RC circuits [7], [8], as schematically shown in Figure 2.

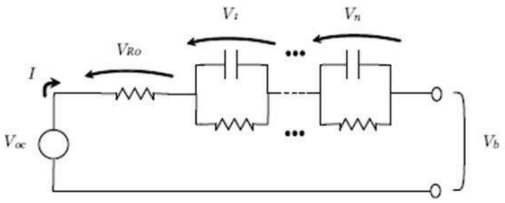

Fig. 2. Scheme of a n^{th} Order Equivalent Circuit Model

The dynamic equation that describes the voltage across the i^{th} RC circuit is given by:

$$\frac{dV_i}{dt} = \frac{1}{R_i C_i} \cdot V_i + \frac{1}{C} \cdot I_{batt} \tag{1}$$

where the parameters are identified based on laboratory test data and are scheduled according to the battery SoC and temperature. Finally, the battery terminal voltage can be expressed as the sum of all the voltage components:

$$V_{batt} = V_{OC} - R_0 \cdot I_{batt} - \sum_{i=1}^{n} V_i + V_h \tag{2}$$

where V_{OC} is the open circuit voltage, and V_h is the hysteresis voltage [7]. The model described above has been validated on a $A123$ $ANR26650$ power cell over a wide range of SoC and temperature, and with the relevant current dynamics experienced in vehicles [8], [9].

B. Battery Thermal Model

The parameters of the electrical model depend on the temperature of the battery cell. However, in [7], [8], the temperature is assumed as a static input to the model. In order to improve the accuracy, a model of the cell temperature dynamics is introduced, based on the work described in [10], [11]. The thermal model is obtained starting from solving a heat diffusion problem for a cylindrical battery cell, subject to internal heat generation and external convective heat transfer at ambient temperature T_{amb}. By applying a model order reduction method in the frequency domain [11], [12], the solution is converted into a linear MISO system in the form:

$$T(s) = \begin{bmatrix} G_{11}(s) & G_{12}(s) \end{bmatrix} \begin{bmatrix} \dot{Q}(s) \\ T_{amb}(s) \end{bmatrix} \tag{3}$$

where $T(s)$ is a spatially-averaged cell internal temperature, $\dot{Q}(s)$ and $T_{amb}(s)$ are the Laplace-transformed heat generation rate and ambient temperature. The heat generation rate is calculated as a function of the cell current, voltage and open circuit voltage:

$$\dot{Q} = I(V_{OC} - V) \tag{4}$$

The transfer functions $G_{i,j}(s)$ of the reduced order model are rational functions as follows:

$$G_{i,j}(s) = K_{i,j} \frac{(s - z_1)(s - z_2)\dots(s - z_{n-1})}{(s - p_1)(s - p_2)\dots(s - p_n)} \tag{5}$$

where n is a finite number and the poles, zeroes and gains are calculated based on the thermal and heat transfer parameters of the cell [11]. For engineering accuracy, a third-order transfer function ($n = 3$) allows one to accurately characterize the frequency response of the system up to $10Hz$, which is the typical sampling frequency adopted for the experimental characterization of battery cells [11], [8].

The cell bulk temperature $T(t)$ is the dynamic variable considered for scheduling the parameters of the electro-thermal battery model. With this approach, the thermal dynamics of the battery is coupled to the electrical dynamics, allowing one to explicitly account for effects related to the electrical load profile and the environmental conditions.

C. Battery Life Estimation Model

In this study, a model-based approach is followed to estimate the battery life under different usage conditions. The approach is based on the weighted Ah-throughput model introduced first in [2] and further developed [3]. The model is based on the concept of accumulated Ah-throughput, implemented through the equation:

$$Ah_{eff} = \int \sigma(T, DoD)|I_{batt}|dt \tag{6}$$

which gives the effective Ah-throughput that the battery can achieve before reaching its end of life, depending on the operating conditions, *i.e.*, temperature and DoD. The nonlinear function $\sigma(T, DoD)$ in Eq. 6, called severity factor map, weights the Ah exchanged by the battery as a function of T and DoD.

The determination of the severity factor surface is typically difficult. For the purpose of this paper, a prototypical example of aging severity factor map was extracted from manufacturer's data, albeit with considerable difficulty as the tests were not necessary conducted with the real driving framework in mind. In the current practice, aging is typically assessed by cycling a cell with 100% DoD at a 1C rate and at near-isothermal conditions. In this paper an estimate of the value of severity factor as a function of operating temperature and DoD is based on available data ([13], [9]) and shown in Figure 3.

On a real vehicle application, though, the actual aging conditions are different from the ones considered to generate the severity factor map. In fact, the battery can operate in a wide range of temperatures and SoC. Hence, the need to conduct an extensive campaign of aging experiments reflecting the actual operation of the battery is unquestionable.

With reference to Figure 3, two regions on the severity factor map are highlighted, namely a fringe spot and a sweet spot. If the battery is operating in a fringe spot, the Ah-throughput model places a relatively high weight to the current exchanged by the battery, hence leading to a decrease in the expected life of the battery.

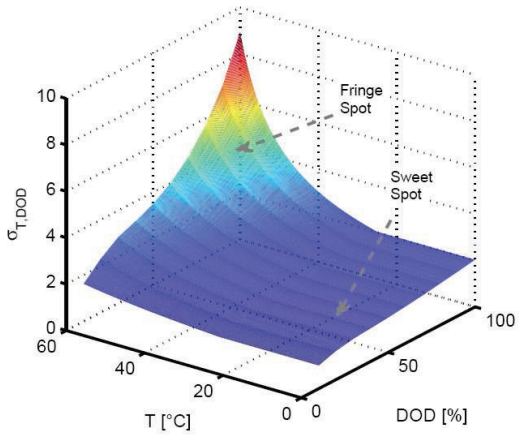

Fig. 3. Severity Factor Map $\sigma(T, DoD)$.

A broad campaign of aging experiments is being conducted at The Ohio State University Center for Automotive Research, to validate the severity map of Figure 3 to reflect the real usage of the battery.

D. Vehicle Model

The battery model is embedded in a PHEV simulator to allow for conducting the simulation study. The simulator builds upon the energy-based model of a conventional hybrid electric vehicle [14], [15], later converted to a PHEV by modifying the battery pack capacity [6]. The selected battery pack allows for an all-electric range (AER) of approximately 30 miles.

The vehicle is based on a series-parallel architecture, which includes a Diesel engine coupled to a Belted Starter Alternator (BSA) on the front axle and an Electric Motor (EM) on the rear axle. Table I describes the main vehicle components. The above configuration allows for a variety of modes such as pure electric drive, electric launch, engine load shifting, motor torque assist, and regenerative braking.

The vehicle simulator is based on a forward-oriented model of the the vehicle longitudinal dynamics. Energy-based models of the vehicle components are present to characterize their energy consumption starting from their respective efficiency maps [16]. The validation of the models was performed first by comparison with laboratory test data on the vehicle components (*e.g.*, engine, transmission electric motors, battery), and then by vehicle data acquisition during driving tests [15].

TABLE I
DESCRIPTION OF THE MAIN VEHICLE COMPONENTS.

Component	Type	Specifications
Chassis	Mid-size SUV	2005 Chevrolet Equinox
Engine	1.9l Diesel	4 Cylinder, 16v, Euro 4, 103 kW @ 4000 rpm, 305 Nm @ 2000 rpm
Belted Starter/ Alternator	Permanent Magnet	Kollmorgen servomotor, 10.6 kW nominal power, 80 Nm peak torque, 4150 r/min Max Speed
Energy Storage	Li-ion Batteries	A123 ANR26650 cells, total capacity 17.2 kWh, 300 V (nominal)
Transmission	6 Speed Automatic	450 Nm torque capacity
Electric Motor	AC Induction	32 kW, 185 Nm peak torque

As a remark, the modular structure of the simulator allows for easily changing various vehicle parameters and components, including battery model, battery size and initial SoC.

E. Vehicle Energy Management Strategy

The supervisory control strategy implemented in the PHEV simulator manages the torque demands to the engine, BSA and rear EM, in order to satisfy the torque required at the wheels.

The control strategy, developed in [6], splits the power demand in order to instantaneously minimize a cost function defined by the cumulative CO_2 emissions:

$$J_{PHEV}(u(t)) = \int_{t_a}^{t_b} \dot{m}_{CO_2,f}(u(t),t) + \dot{m}_{CO_2,e}(u(t),t)dt \tag{7}$$

where $\dot{m}_{CO_2,f}$ is the mass flow rate of the CO_2 produced by the engine and $\dot{m}_{CO_2,e}$ is the mass flow rate of CO_2 produced as result of the electric energy on-board consumed. While the former term is directly related to the engine brake specific fuel consumption map, the latter is a more complex function, which depends on the battery energy utilization and by the specific CO_2 emissions of the grid energy generation mix, estimated using the GREET model [17].

Because the overall (fuel and grid) CO_2 emissions are considered in the cost function, the effect of the vehicle to grid interactions are explicitly accounted for on the vehicle energy utilization.

With reference to the power flow of the vehicle model shown in Fig. 4, the control variable $u(t)$ for the considered problem is a two-dimensional vector defined as:

$$u(t) = [P_{batt}; P_{EM,el}/P_{batt}] \tag{8}$$

where the first element is the total battery power and the latter represents the power split between the rear electric motor and the BSA. According to the power flow of the vehicle powertrain, it is possible to state the following balances:

$$\begin{aligned} P_{tot}(t) =& P_{ICE}(t) + P_{BSA,el} \cdot \eta_{BSA} + P_{EM,el} \cdot \eta_{EM} \\ P_{batt}(t) =& P_{BSA,el} + P_{EM,el} \end{aligned} \tag{9}$$

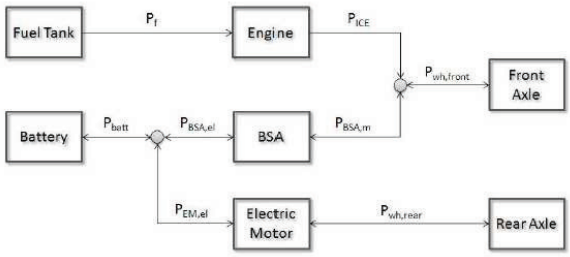

Fig. 4. Block Diagram of the Vehicle Power Flows.

where $P_{tot}(t)$ is the total power request to the hybrid driveline, and $P_{tot} = P_{wh,front} + P_{wh,rear}$.
The control and state variables are subject to constraints in order to respect limitations from the drivetrain components and for safe vehicle operations. In particular, the battery SoC (in principle defined between zero and one) is usually limited in order to avoid operating conditions that may result in battery abuse and premature aging:

$$SoC_{min} \leq SoC(t) \leq SoC_{max} \tag{10}$$

Further constraints may posed by the components of the drivetrain, which are typically subject to power limitations:

$$\begin{aligned} P_{batt,min} \leq & P_{batt}(t) \leq P_{batt,max} \\ P_{EM,min} \leq & P_{EM}(t) \leq P_{EM,max} \\ P_{BSA,min} \leq & P_{BSA}(t) \leq P_{BSA,max} \end{aligned} \tag{11}$$

Details on the supervisory controller algorithm are provided in [6], and in particular, the mathematical expression of $\dot{m}_{CO_2,e}$ in Equation (7). Here, a calibration parameter is defined in order to privilege the utilization of the electric energy over the fuel. This parameter allows one to define the operating mode of the vehicle and the discharging rate of the battery during vehicle operations, as documented by the results reported in [6].

III. Simulation and Analysis of Results

The electro-thermal battery model, together with the life estimation model, was integrated into the PHEV simulator and the supervisory controller to build a framework for deterministic and stochastic simulations. This paper reports the preliminary results of the simulation study, focusing on the effects of the PHEV control parameters on the battery estimated life.

A full factorial DOE of two variables was considered to evaluate the effects of the vehicle operating modes (charge depleting or charge sustaining), and the constraints on the battery SoC bounds. Specifically, a set of simulations was performed considering constant ambient temperature ($T_{amb} = 25°C$), and a fully charged battery at the beginning of each driving schedule. Furthermore, the simulation results presented are based on a real-world driving cycle obtained from a fleet study. The driving schedule considered, shown in Figure 5, is representative of a typical commute from home to work, which includes both urban and highway segments.

In order to allow for the supervisory controller to deplete the battery, it is important that the driving cycle length is greater than the AER. In this case, three repetitions of the cycle shown in Figure 5 were considered in the following simulations.

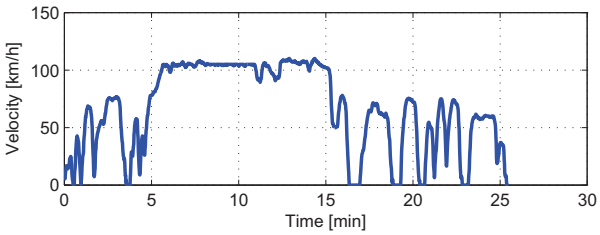

Fig. 5. Velocity Profile of the Driving Schedule Considered for the Simulation Study.

While the upper SoC bound was set to 0.90 of the total battery capacity, the lower SoC bound was a variable for the aging evaluation. In this preliminary study, five levels of the lower SoC bound were considered, between 0.10 and 0.30 of the battery capacity. x Furthermore, two different energy management strategies have been considered to deplete the battery at different rates, indicated in Figure 6 as Charge Depleting-Charge Sustaining (*CD-CS*) mode, and Blended Mode (*Blended*). The figure shows an example of the SoC profile for the two operating modes, for a fixed SoC lower bound at 0.20. When the supervisory controller operates the vehicle in Blended Mode, the lower SoC bound is reached only at the end of the driving pattern, whereas in CD-CS mode the controller will attempt at depleting the battery to the lower SoC bound in the shortest time possible, thereafter switching to charge sustaining mode.

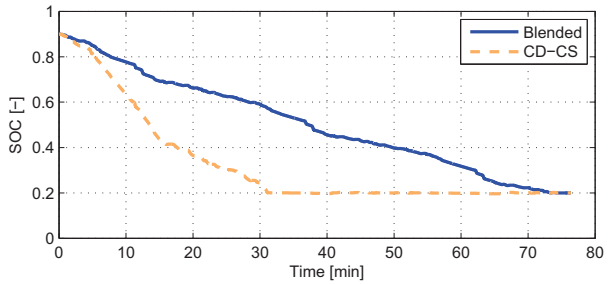

Fig. 6. SoC Profile in Blended Mode and CD-CS Mode (SoC Lower Bound Set at 0.20).

The percentage of driving cycle operated in charge sustaining mode at the lower SoC bound was considered as the second variable for the DOE study. Note that, in this case, such variable can not be set directly, as its value depends on the characteristics of the driving cycle and on the parameter of the PHEV supervisory controller [6].

It is evident that the fraction of driving cycle operated in CS mode reaches a limit of zero if the vehicle is operated in blended mode. Varying the duration of the charge sustaining

mode has an immediate impact on the effective Ah-throughput of the battery. In particular, the CD-CS mode represents a worst-case scenario where the controller will initially attempt at depleting the battery in a relatively short time, in relation with the imposed driving pattern. During the initial discharging phase, the C-rate will reach high peak values, which will increase the heat generation rate and, ultimately, the battery temperature. Consequently, the battery will experience more severe conditions, drawing up the fringe spot region in the severity factor map shown in Figure 3.

The behavior described above is summarized in Figure 7, where the statistical distribution of the C-rate in CD-CS mode is represented, with a SoC lower bound of 0.20. When the vehicle is operated in charge depleting mode (left plot), high C-rates peaks are reached, in some cases up to 14C. However, the distribution of the C-rate evidences that the battery is mostly depleted at rates below 5C, with an average rate of discharge around 1.35C. Once the lower SoC bound is reached, the controller operates the vehicle in charge sustaining mode; here, as shown in the right plot, the mean C-rate is zero with minimal dispersion of the data.

It is worth observing that the results shown in Figure 7 justify the assumption of neglecting the effects of the C-rate on the severity factor, hence considering only the dependence on temperature and DoD.

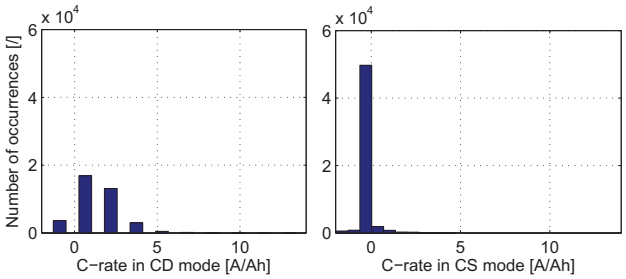

Fig. 7. Distribution of the C-Rate During CD-CS Mode (SoC Lower Bound Set at 0.20).

The results of the DOE are summarized in Table II, reporting the main model outputs for three different values of the SoC lower bound. For each SoC value, the results are reported with reference to the blended mode and the CD-CS mode, respectively.

Although the maximum C-rate never exceeds 14C, the average battery power demand increases substantially when the lower SoC bound is decreased. This has direct consequence on the battery cell temperatures, which tend to increase despite imposing constant ambient temperature.

Table III shows the weighted cumulative Ah-throughput and the cumulative Ah (*i.e.*, computed considering the actual battery current) at the end of the simulated driving cycle, varying the PHEV control parameters. The weighted cumulative Ah-throughput is the output of the life estimation model, calculated through the severity factor map shown in Figure 3 [3]. The tabulated results are shown graphically in Figures 8-9, providing an intuitive representation of the cumulative battery damage that stems from the different DoD levels and vehicle operation modes.

By comparing the results, it is possible to observe that the damage accumulation, which influences the battery life expectation, increases as the lower SoC bound is decreased. This behavior is common to both vehicle operating modes.

TABLE II
SUMMARY OF SIMULATION RESULTS.

SoC limit	**0.10**		**0.20**		**0.30**	
Mode	**blended**	**cd-cs**	**blended**	**cd-cs**	**blended**	**cd-cs**
C-rate$_{med\ cd}$ [1/h]	0.57	1.43	0.52	1.35	0.45	1.11
C-rate$_{med\ cs}$ [1/h]	-	0.00	-	0.00	-	0.00
C-rate$_{max}$ [1/h]	10.92	13.79	10.28	13.78	10.92	13.79
P$_{med}$ [kW]	9.51	10.31	8.59	9.04	7.54	7.33
P$_{max}$ [kW]	184.40	212.30	169.40	212.10	137.80	204.00
T$_{med}$ [°C]	27.9	28.6	26.7	27.6	26.2	27.2
T$_{max}$ [°C]	27.7	31.4	27.6	30.9	27.1	30.8

TABLE III
SUMMARY OF CUMULATIVE AND WEIGHTED CUMULATIVE AH-THROUGHPUT.

SoC limit	**0.10**		**0.20**		**0.30**	
Mode	**blended**	**cd-cs**	**blended**	**cd-cs**	**blended**	**cd-cs**
Ah	52.02	53.52	46.19	47.42	39.82	41.81
Weighted Ah	81.86	89.26	69.52	75.61	57.20	64.05

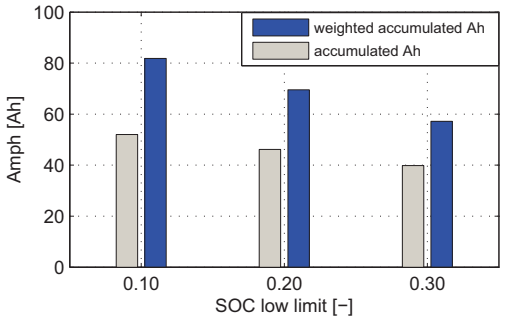

Fig. 8. Summary of Ah-Throughput and Weighted Ah-Throughput in Blended Mode.

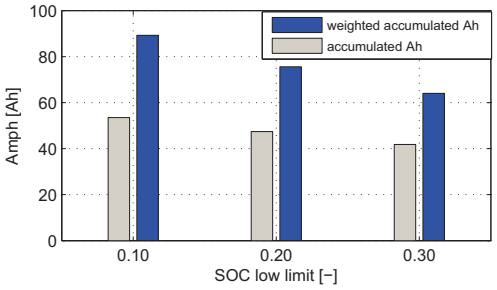

Fig. 9. Summary of Ah-Throughput and Weighted Ah-Throughput in CD-CS Mode

The simulation results obtained illustrate the presence of a linear relationship between the variation of the weighted Ah-throughput (with respect to the accumulated Ah) and the lower SoC bound, for both PHEV operating modes. In particular, by discharging the battery up to a SoC bound of 0.10 leads to an increase in weighted Ah greater than 10%, in comparison with a SoC bound of 0.30.

Furthermore, the observed increase is almost doubled when the PHEV is operated in CD-CS mode. As regards the absolute Ah values reported in Table III, it can be noticed that when the SoC lower bound of 0.30 is reached only at the end of the cycle, therefore no charge sustaining operations are present, the weighted Ah-throughput achieves a value that is much lower (more than 30%) than the one resulting from a CD-CS cycle.

When the battery is slowly depleted during the cycle (in Blended mode), the severity factor obtained (as a function of temperature and DoD) results lower than in CD-CS mode. This behavior is shown in Fig. 10, relative to a lower SoC bound of 0.20. The severity factor values obtained in Blended mode populate the severity map area close to the sweet spot, hence maintaining the estimated battery life very close to the manufacturer's specifications.

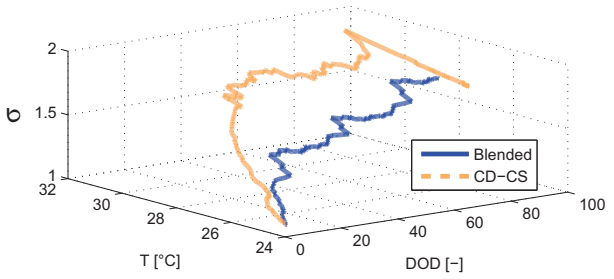

Fig. 10. Severity Factor Profiles as a Function of DoD and Temperature During Blended and CD-CS Mode (SoC Lower Bound Set at 0.20).

IV. Conclusion

This paper describes the preliminary results of a comprehensive simulation study on the characterization of Li-ion battery aging factors for PHEV applications. A model-based methodology that estimates the battery residual life under real-world driving conditions is developed, based on a modeling framework that integrates an electro-thermal battery model, a life estimation model, and a PHEV forward-oriented model including a supervisory energy management strategy.

A design of experiments was defined and conducted in simulation to identify the effects of the PHEV supervisory controller on the battery life. In particular, a direct relationship was observed between the damage accumulation that influences the battery life and the rate of battery discharging during the duty cycle. In Charge Depleting-Charge Sustaining mode, the battery is subject to high DoD rates, which increase the heat generation rate and ultimately the pack temperature. Such effects are compounded when the severity factor is calculated, resulting in a significantly higher values of the weighted Ah-throughput. Similarly, a correlation between the weighted accumulated Ah and the lower bound on the battery SoC was observed.

A more thorough investigation of the root causes for battery aging on PHEVs is currently under way. The developed modeling framework will be used to explore large-scale PHEV simulations, to study the effects of a wide range of design, environmental and control variables on battery life. Among others, PHEV battery sizing, charging patterns and daily/seasonal/geographical temperature variations will be included in the analysis, based on a stochastic mix of real driving scenarios obtained from on-going fleet studies.

V. Acknowledgements

The work described in this paper was supported by the CAR Industrial Consortium.

References

[1] A. Pesaran, K. Smith, and T. Markel, "Impact of the 3Cs of Batteries on PHEV Value Proposition: Cost, Calendar Life, and Cycle Life," *Proc. of Advanced Automotive Battery Conference*, 2009.

[2] L. Serrao, S. Onori, and G. Rizzoni, "A Novel Model-Based Algorithm for Battery Prognosis," *Proc. of IFAC SAFEPROCESS*, 2009.

[3] P. Spagnol, S. Onori, V. Marano, Y. Guezennec, and G. Rizzoni, "A Life Estimation Method for Lithium-ion Batteries in Plug-in Hybrid Electric Vehicles Applications," *International Journal of Power Electronics, Special Issue (To Appear)*, 2010.

[4] A. Pesaran, T. Markel, H. Tataria, and D. Howell, "Battery Requirements for Plug-In Hybrid Electric Vehicles - Analysis and Rationale," *Proc. of International Electric Vehicle Symposium*, 2007.

[5] P. Spagnol, S. Onori, N. Madella, Y. Guezennec, and J. Neal, "Aging and Characterization of Li-Ion Batteries in a HEV Application for Lifetime Estimation," *Proc. of IFAC Symposium Advances in Automotive Control*, 2010.

[6] S. Stockar, V. Marano, G. Rizzoni, and L. Guzzella, "Optimal Control for Plug-in Hybrid Electric Vehicles Applications," in *Proc. of American Control Conference*, 2010.

[7] Y. Hu, S. Yurkovich, Y. Guezennec, and R. Bornatico, "Model-Based Calibration for Battery Characterization in HEV Applications," in *Proc. of American Control Conference*, 2008.

[8] Y. Hu, B. J. Yurkovich, S. Yurkovich, and Y. Guezennec, "Electro-Thermal Battery Modeling and Identification for Automotive Applications," in *Proc. of ASME Dynamic Systems and Control Conference*, 2009.

[9] A123-High Power Lithium Ion ANR26650M1A - Datasheet Specs, *www.A123systems.com/cms/product/pdf/1/ANR26650M1A.pdf*.

[10] M. Muratori, M. Canova, Y. Guezennec, and G. Rizzoni, "A Reduced-Order Model for the Thermal Dynamics of Li-Ion Battery Cells," *Proc. of the IFAC Symposium in Advances in Automotive Control*, 2010.

[11] M. Muratori, N. Ma, M. Canova, and Y. Guezennec, "A Model Order Reduction Method for the Temperature Estimation in a Cylindrical Li-ion Cell," *Proc. of the ASME Dynamic Systems and Control Conference*, 2010.

[12] H. Khalil, *Nonlinear systems*. Prentice Hall, 1996.

[13] T. Markel and A. Simpson, "Plug In Electric Vehicle Energy Storage System Design," in *Proc. of Advanced Automotive Battery Conference*, 2006.

[14] M. Arnett, K. Bayar, C. Coburn, Y. Guezennec, K. Koprubasi, S. Midlam-Mohler, K. Sevel, M. Shakiba-Herfeh, and G. Rizzoni, "Cleaner Diesel Using Model-Based Design and Advanced Aftertreatment in a Student Competition Vehicle," *SAE Technical Paper 2008-01-0868*, 2008.

[15] K. Koprubasi, "Modeling and Control of Hybrid-Electric Vehicle for Drivability and Fuel Economy Improvements," Ph.D. dissertation, The Ohio State University, 2008.

[16] L. Guzzella and A. Sciarretta, *Vehicle Propulsion Systems: Introduction to Modeling and Optimization*. Springer Verlag, 2007.

[17] Argonne National Laboratory, "Greet 1.8b," 2008.